ACS APPLIED MATERIALS & INTERFACES

Research Article

www.acsami.org

Surface Double Phase Network Modified Lithium Rich Layered Oxides with Improved Rate Capability for Li-Ion Batteries

Lichao Guo,[†] Naiqin Zhao,*[,†,‡] Jiajun Li,[†] Chunnian He,[†] Chunsheng Shi,[†] and Enzuo Liu*[,†,‡]

[†]School of Materials Science and Engineering and Tianjin Key Laboratory of Composites and Functional Materials, Tianjin University, Tianjin 300072, China

[‡]Collaborative Innovation Center of Chemical Science and Engineering, Tianjin 300072, China

Supporting Information

ABSTRACT: Poor rate capability and cycling performance are the major barriers to the application of lithium rich layered oxides (LLOs) as the next generation cathodes materials for lithium-ion batteries. In this paper, a novel surface double phase network modification has been applied to enhance the rate property of $Li_{1.2}Co_{0.13}Ni_{0.13}Mn_{0.54}O_2$ (LR) via flexible electrostatic hetero-coagulation and thermal treatment. The template action of multiwalled carbon nanotubes (MWCNTs) network on LR clusters results in the spinel phase network formation at the interface between the LR and MWCNTs. The phase transformation process from layered component toward spinel phase is identified through the detailed investigation of the interface using high-resolution transmission electron microscopy, fast Fourier transformation, and the detailed analysis on the transformation of simulated diffraction patterns. The double phases stretch two sets of networks with both fine Li ion and electron conductivity onto and within the clusters of LR, lowering the surface resistance, reducing the electrochemical polarization, and as a result, significantly enhancing the rate capability of LR. The double phase network modification, combining MWCNT coagulation and spinel phase modification, has profound potential in accelerating kinetics for LLOs.

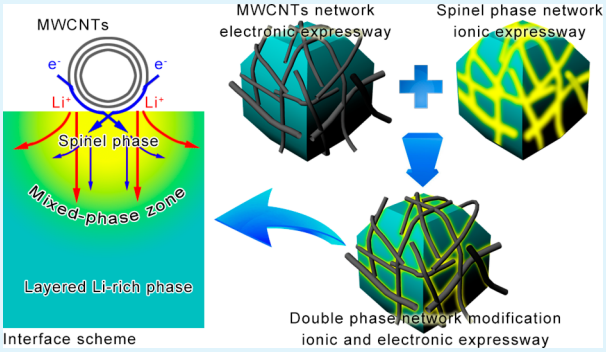

KEYWORDS: *surface modification, lithium rich layered oxides, double phase network, rate capability*

1. INTRODUCTION

With the increasing demand for clean and sustainable energy all over the world, power sources for high energy storage are being investigated at an increasing rate. Lithium-ion batteries (LIBs), as one of the main power sources for portable electronics and back-up power devices, have the advantages of high energy density, high working voltage, and flexible design.[1−3] Nowadays, despite the suitability for the small-scale devices, LIBs cannot support the plug-in hybrid-electric vehicles and all-electric vehicles, due to their insufficient energy density or working life.[4] Thus, it becomes a considerable issue to investigate materials with high energy density and power density for LIBs.

Li_2MnO_3·$LiMO_2$ (M = Co, Ni, Mn), the lithium rich layered oxides, are becoming the ideal high-energy-density cathode materials because of their high theoretical capacity (>250 mAh/g), good thermal stability, and low cost.[2,5] The two phases, layered Li_2MnO_3 and $LiMO_2$ (M = Ni, Co, Mn), are closely integrated into each other on the nanoscale level. Charged above 4.5 V, two lithium ions are removed from the Li_2MnO_3 component with one oxygen ion irreversibly released; yet only one lithium ion can return in the following discharge process, causing irreversible capacity loss.[6] In addition, the electrolyte reacts with the trace water into other chemicals under such a high voltage, damaging the surface structure of lithium rich layered oxides and blocking the transfer of lithium ion and electron. As a consequence, the byproducts immensely affect the cycling performance and rate capability. Last but not least, the poor conductivity of Li_2MnO_3 results in the rate capability rather undesirable for practical usage.

Therefore, numerous research efforts are focused upon improving the cycling performance and rate capability of lithium rich layered oxides. One strategy is surface coating with ionic conductive materials.[7−11] For instance, a double-layer surface modified $Li[Li_{0.2}Mn_{0.54}Ni_{0.13}Co_{0.13}]O_2$ cathode with an improved rate capability was proposed,[12] and the modified samples deliver a discharge capacity of more than 200 mAh/g at 2C. Spinel coating on the particles of lithium rich spinel/layered materials via a simple "dip and dry" process results in a better rate electrochemical property.[13] Modification with a carbon source is another crucial strategy.[14−18] Deng et al.[19] modified the $Li_{1.2}Co_{0.13}Ni_{0.13}Mn_{0.54}O_2$ with PVP by a liquid phase method, mainly contributing to the cycling performance. Recently, Song et al.[20] successfully wrapped lithium rich

Received: September 17, 2014
Accepted: December 12, 2014
Published: December 12, 2014

DOI: 10.1021/am506354e
ACS Appl. Mater. Interfaces 2015, 7, 391−399

materials with graphene by a simple chemical method, achieving a capacity more than 150 mAh/g under 10C. For optimizing the modification (coating) structure, the concept of "hybrid coating" with both good Li^+ and electron conductivity is proposed.[17]

Carbon has been demonstrated to induce phase transformation from the two-dimensional (2D) layered structure to the three-dimensional (3D) spinel structure.[20,21] In addition, the carbon nanotubes (CNTs), with excellent electron conductivity, have been used as an electronic conduction network in different kinds of materials. For example, $LiNi_{0.4}Mn_{0.4}Co_{0.2}O_2$ with single-walled carbon nanotubes has a durable high-rate capability.[22] Therefore, CNT-modified lithium rich layered oxides may achieve the multifunction of hybrid modification.

Still, the problems of homogeneous dispersion of CNTs and good contact between CNTs and lithium rich layered oxides exist. The ideal combination of CNTs and cathode materials is that CNTs grow directly on the surface of the active materials with the help of catalysts. However, most in situ growth of CNTs requires a reductive process for catalysts, while lithium rich layered oxides demand a highly oxidative environment. It is necessary to choose an ideal method that can bypass the problem. Electrostatic heterocoagulation provides us a physical method to combine ex situ CNTs with lithium rich layered oxides. Generally, during electrostatic heterocoagulation, the environment factor, such as pH, is set within a specific range to allow two kinds of particles gaining the same ζ-potential, so that the particles absorb onto one another.[23−26] With the concentration increment rate controlled, CNTs are expected to disperse onto the surface of active materials with good contact.

In this study, we have successfully modified the lithium rich materials with homogeneous double phase networks using MWCNTs via a facile electrostatic heterocoagulation and thermal treatment method. With the short thermal treatment under the protection of argon atmosphere, MWCNTs not only adhere closely to the clusters of the active materials physically but also chemically react with the cathode surface to produce the 3D spinel lithium manganese phase, improving both ion diffusion coefficient and electron conductivity. The double phase network modification leads to the great optimization of high rate performance of lithium rich materials. Phase transformation process within the interface between MWCNTs and lithium rich layered oxides is analyzed in detail, and a schematic diagram is presented to illustrate the mechanism.

2. EXPERIMENTAL SECTION

2.1. Synthesis of Double Phase Network Modified $Li_{1.2}Co_{0.13}Ni_{0.13}Mn_{0.54}O_2$. $Li_{1.2}Co_{0.13}Ni_{0.13}Mn_{0.54}O_2$ (LR) was synthesized via a sol gel method, using citric acid as chelating agents. 2 wt % of excess $LiNO_3$ was used to compensate for the loss of lithium salt during calcination. Stoichiometric amounts of $Ni(NO_3)_2{\cdot}6H_2O$, $Co(NO_3)_2{\cdot}6H_2O$, $Mn(Ac)_2{\cdot}4H_2O$, and $LiNO_3$ were dissolved in deionized (DI) water simultaneously. The molar ratio of citric acid $Li_{1.2}Co_{0.13}Ni_{0.13}Mn_{0.54}O_2$ was 1:1. The citric acid aqueous solution was added dropwise to the mixed salt solution mentioned above. Then ammonium hydroxide was added dropwise until the solution pH was adjusted to around 7.5. The solution was evaporated at 80 °C in water bath with continuous magnetic stirring until colloidal gel was obtained. The gel was heated at 120 °C in a vacuum oven for 24 h. The dried precursor was then precalcined in the chamber furnace at 450 °C for 3 h. The target compound was obtained by sintering at 850 °C for 16 h in air and then quenching on a copper plate in room temperature. The pure $Li_{1.2}Co_{0.13}Ni_{0.13}Mn_{0.54}O_2$ (P-LR) was obtained.

MWCNTs were acid treated in a mixture of nitric and sulfuric acid (volume ratio, 1:2) for 5 h under continuous stirring, and then filtered with DI water until the pH of filtrate was adjusted to 7.0−7.8. Electrostatic heterocoagulation has been realized using acid treated MWCNTs.[25] 10 wt % of gelatin was dissolved in 40 mL of hot DI water and a specific amount of LR was added. The mixture was filtered and dried at 100 °C overnight. The acid treated MWCNTs aqueous suspension was added into the gelatin-coated LR aqueous suspension drop by drop. Two drops of acetic acid was added in the mixed suspension to get to the isoelectric point for gelatin-coated LR and acid treated MWCNTs. Vigorous stirring proceeded throughout the electrostatic heterocoagulation process for 5 h. The suspension was filtered using DI water, and the as-prepared powder was dried at 80 °C in a vacuum oven for 2 h. The powder was finally heated at 300 °C for 0.5 h under Ar atmosphere. The double phase network modified LR was obtained. In section 3, $Li_{1.2}Ni_{0.13}Co_{0.13}Mn_{0.54}O_2$ modified by x % MWCNTs in weight are abbreviated as "x" %MCNT-LR" with "x" equal to 5, 10, 15, or 20.

2.2. Characterization. The microscopic morphology of as-prepared samples were observed by a field emission scanning electron microscopy (FESEM, Hitachi-S4800) instrument operated at 5 kV. Detailed morphology and lattice structure were observed by a high-resolution transmission electron microscopy (HR-TEM, JEM-2100F) instrument with an accelerating voltage of 200 kV. All the TEM samples were prepared by depositing a drop of diluted suspension in ethanol on an ultra-thin-carbon-film-coated copper grid. The crystalline phase analysis was carried out by a powder X-ray diffraction system (XRD, Bruker ADVANCE D8, Cu Kα radiation, wavelength Kα_1 0.154 056 nm, Kα_2 0.154 439 nm) at room temperature. Raman spectra were obtained via a Renishaw Raman spectroscopy system. The laser wavelength was 532 nm.

2.3. Electrochemical Measurements. The electrode was prepared with a mixture of active material, carbon black, and polyvinylidene fluoride binder dissolved in *N*-methyl-2-pyrrolidone solvent at a weight ratio of 80:10:10. The well mixed slurry was coated on an aluminum foil current collector using an I-type scraper, dried at 120 °C overnight in a vacuum oven, and cut into a disk with a diameter of 12 mm. Then the CR2032-type half coin cells were assembled in a Ar-filled glovebox (Etelux LAB2000) using lithium metal as the counter electrode and reference electrode and 1 M $LiPF_6$ dissolved in ethylene carbonate (EC)/ethyl methyl carbonate (EMC)/dimethyl carbonate (DEC) (1:1:1 in volume) as the electrolyte. Galvanostatic charge/discharge tests were performed in a voltage range of 2.0−4.8 V with different current densities using Land battery testers (Land CT2001A). For the cycling test, the half coin cells were charged and discharged between 2.0 and 4.8 V at increasing rates of 0.05C, 0.1C, and 0.2C for the first three cycles. From the 4th cycle, the half cells were cycled at the current rate of 0.5C to test the cycling performance. The cyclic voltammetry (CV) tests were conducted using a CHI 660D electrochemical workstation between 2.0 and 4.8 V versus Li^+/Li at a scan rate of 0.2 mV s^{-1} at room temperature. The electrochemical impedance spectroscopy (EIS) of the cells was conducted on an electrochemical workstation (Autolab PGSTAT302N) with a frequency range of 10 mHz−100 kHz.

3. RESULTS AND DISCUSSION

3.1. Identification of Double Phase Modification. Figure 1 shows the FESEM images of LR before and after surface modification with MWCNTs. In Figure 1a,b, P-LR consists of particles in the shape of regular and irregular polyhedrons with crystal sizes of 100−200 nm. No substantial difference can be observed in particle size and shape between P-LR (Figure 1b) and 10%MCNT-LR samples (Figure 1d). MWCNTs homogeneously coagulate on the clusters of LR (Figure 1c,d,e,f). The well coagulated MWCNTs stretch a fine network onto LR, in favor of the electronic conduction. The close contact between MWCNTs and LR has been further confirmed by TEM in Figure S1 (Supporting Information).

DOI: 10.1021/am506354e
ACS Appl. Mater. Interfaces 2015, 7, 391−399

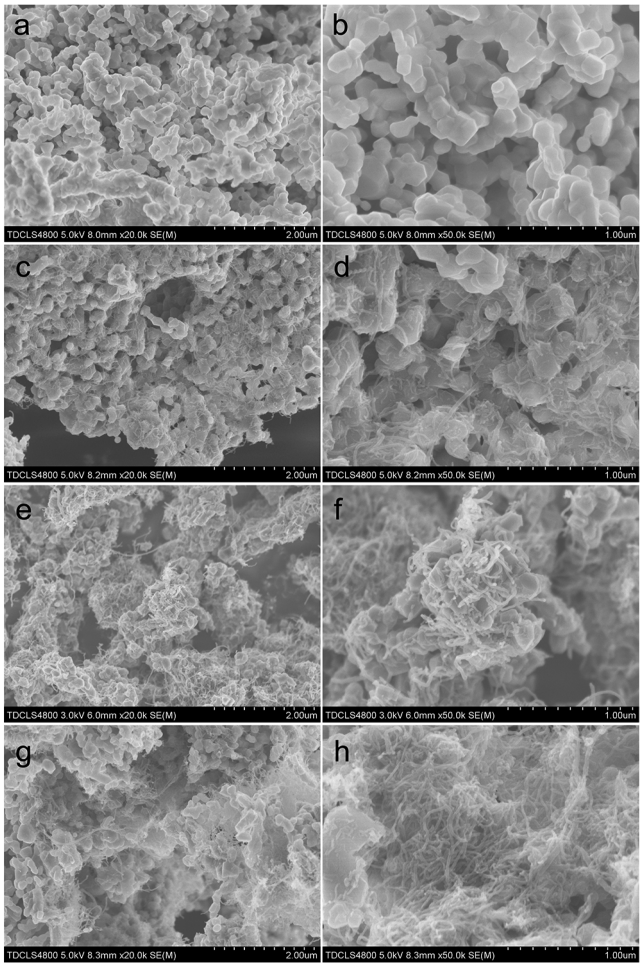

Figure 1. FESEM images of the as-prepared LR samples before and after modification. (a, b) P-LR; (c, d) 10%MCNT-LR; (e, f) 15% MCNT-LR; (g, h) 20%MCNT-LR.

After an ultrasonic procedure for TEM sample preparation, MWCNTs can still closely adhere to the LR particles. When the mass fraction of MWCNTs rises up to 20%, excess MWCNTs continue coagulating on the modification structure. The particles of LR can hardly be found in Figure 1g,h. The excess MWCNTs extend a thick coating that seals the electrochemically active LR materials and prolongs the path of lithium transfer from the electrolyte to the cathode materials. Meanwhile, the tightly joint MWCNTs rapidly decrease the exposed area of surface region for lithium intercalation and deintercalation, which is predicted to impose negative effect on the electrochemical performance. Moreover, too much MWCNTs will reduce the specific capacity of the modified samples. In brief, by controlling the content of MWCNTs (10–15 wt %), homogeneous contacts between MWCNTs and LR can be realized via electrostatic coagulation method.

XRD patterns of LR before and after modification are shown in Figure 2. All XRD patterns can be finely indexed to the α-$NaFeO_2$ layered structured $LiNiO_2$ belonging to the space group $R\bar{3}m$ (trigonal symmetry), except for the weak peaks between 20 and 24°. The weak peaks can be specifically indexed as (002) and (110), which are due to the $LiMn_6$ cation ordering (Figure 2a inset), revealing the superlattice structure in the layers of Li_2MnO_3, space group $C2/m$ (monoclinic symmetry).[27−29] For the modified samples, the peak at around

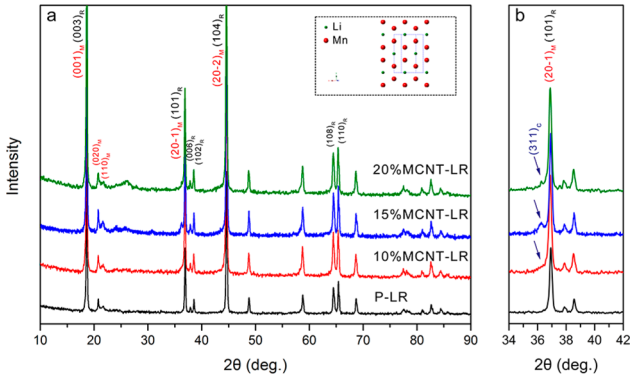

Figure 2. (a) Overall and (b) partially close-up XRD patterns of the as-prepared LR samples before and after double phase modification. Subscript R refers to space group $R\bar{3}m$, the layered trigonal phase. Subscript M refers to space group $C2/m$, the layered monoclinic phase. Subscript C refers to space group $Fd\bar{3}m$, the spinel cubic phase. The inset shows the $LiMn_6$ cation arrangement in the layered Li_2MnO_3 phase.

26.4°, observed in 15%MCNT-LR and 20%MCNT-LR patterns, gets stronger as the CNTs contents increase, which is indexed to the graphite-like (002) plane.

For the modified samples, the peak at 36.5° (blue arrows) can be indexed neither to the $R\bar{3}m$ space group nor to $C2/m$. To compare with PDF card, this weak peak is indexed to the spinel lithium manganese oxides ($Fd\bar{3}m$), the (311) lattice plane. Moreover, XRD patterns of the P-LR with thermal treatment and 15%MCNT-LR before thermal treatment have no peak at 36.5° (Figure S2, Supporting Information), indicating that the phase transformation is due to both the existence of MWCNTs and thermal treatment. MWCNTs impose chemical reduction impact on the surface region of lithium rich layered oxides during the thermal treatment procedure, resulting in the formation of 3D spinel phase.[20,21,30,31] Even so, the observed peak for spinel phase is not strong, revealing that the reduction effect is too weak to change all the crystal lattice of LR particles owing to the relatively low temperature and short time in thermal treatment process. The phase transformation has been corroborated using Raman spectroscopy as well (see Figure S3 in the Supporting Information). The spinel component has a 3D structure favorable for lithium-ion transfer;[4,13] thus, MWCNTs combined with spinel phase region will undoubtedly lower the surface resistance.

The cyclic voltammograms (CV) of LR samples before and after surface modification also indicate the existence of the spinel phase. In Figure 3a, the first anodic peak of the CV profile appears at around 4.1 V, associated with Ni from Ni^{2+} to Ni^{4+}. The first anodic peak remains almost the same in the following cycling process due to the reversibility. The broad second anodic peak at above 4.5 V is predominately due to the electrochemical activation of Li_2MnO_3, with irreversible loss of Li_2O from Li_2MnO_3 crystal structure. Meanwhile the cobalt oxidation from Co^{3+} to Co^{4+} can proceed above 4.5 V.[32] The broad second anodic peak only appears in the first cycle because of the irreversible reaction. For the reduction part, Co^{3+}/Co^{4+}, $Ni^{2+}/Ni^{3+}/Ni^{4+}$, and Mn^{3+}/Mn^{4+} reduction reactions are reflected in the peaks at 4.3, 3.6, and 3.1 V, respectively.[32] It is worth noting the small anodic peak (marked by "o") at 3.0 V and cathodic peak (marked by "*") at 2.6 V in Figure 3b,c. The featured peaks appear in the first cycle and

DOI: 10.1021/am506354e
ACS Appl. Mater. Interfaces 2015, 7, 391−399

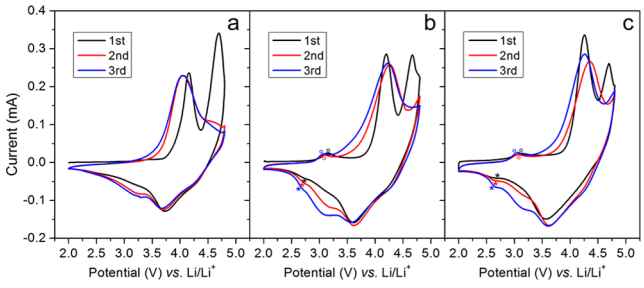

Figure 3. Cyclic voltammograms for the as-prepared LR samples before and after double phase modification. (a) P-LR, (b) 10%MCNT-LR, (c) 15%MCNT-LR.

remain almost the same intensity in the following two cycles, which are due to the surface spinel phase.[34]

XRD patterns, Raman spectrum, and CV profiles all demonstrate the existence of spinel phase, which is yielded by the chemical reaction between MWCNTs and the LR particles. Further proof of double phase (MWCNTs and spinel phase) modification will be discussed in section 3.2.

3.2. Surface and Interface Analysis. LR particles are highly crystallized, and the lattice can be easily identified in high-resolution transmission electron microscopy (HR-TEM) images and selected area diffraction (SAED) patterns of the surface area of P-LR before electrochemical cycling (Figure 4).

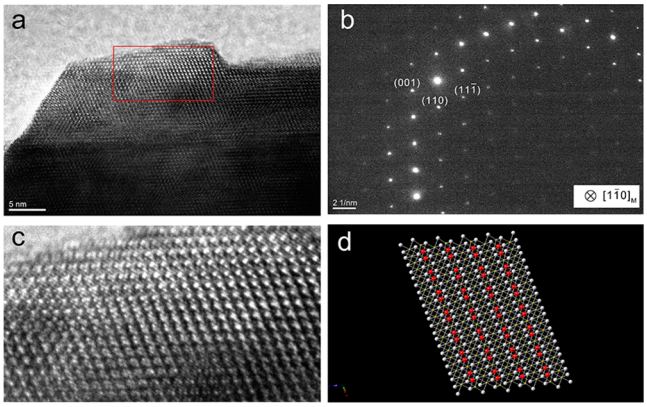

Figure 4. (a) High-resolution transmission electron microscopy (HR-TEM) images for P-LR before cycling, (b) selected area diffraction (SAED) patterns, (c) the magnification image of red box region of (a), and (d) the simulated lattice of Li_2MnO_3 from the specific zone axis $[1\ \bar{1}\ 0]_M$. Red, white, and yellow spheres represent Mn, O, and Li atoms, respectively.

Figure 4a corresponds to the monoclinic *C*2/*m* lattice along the $[1\ \bar{1}\ 0]_M$ zone axis. The particle ends with rough edges. Based on the lattice and diffraction patterns (Figure 4b), the crystal structure is simulated (Figure 4d), which can perfectly match with the magnified lattice in Figure 4c on the atomic scale. The 2D layered structure is displayed from the $[1\ \bar{1}\ 0]_M$ zone axis, and lithium will have to deintercalate from or insert into the crystal lattice along (001) plane during charging or discharging processes. The diffusion coefficient $D(Li^+)$ for Li rich layered cathodes is only 10^{-16} to 10^{-14} $cm^2 \cdot s^{-1}$,[35] accounting for the poor rate capability of lithium rich layered oxides. Other surface regions of P-LR are shown in Figures S4 and S5 (Supporting Information). Crystal information has been examined by fast Fourier transform (FFT) for the corresponding region. It is revealed that the Li_2MnO_3 component is prone to forming on the surface region since the diffraction patterns for $LiMO_2$ (M = Ni, Co, Mn) can hardly be observed at the surface area. As is reported, the slow kinetics in nanostructured cathodes is largely due to high surface resistance resulting from the substantial barriers for lithium diffusion and electron transfer.[36] The segregation of Li_2MnO_3 component results in the substantial barriers at the surface region, and thus, poor rate property of pure LR is obtained.

HR-TEM images of the interfaces between MWCNTs and LR particles are presented in Figures 5 and 6. As shown in Figure 5, the lattice arrangement at the interface is extremely different from that at the particle inner. From regions A to B and then to C (red box) in Figure 5a, the FTT patterns change with the lattice transformation from layered Li_2MnO_3 to spinel $LiMn_2O_4$. Region B shows two sets of diffraction patterns combined, corresponding to the mixed phase transforming zone. In Figure 5b, the simulated ideal diffraction patterns can perfectly match with the FTT images. It shows that monoclinic $(1\ 1\ \bar{2})_M$ plane is parallel to spinel $(1\ \bar{4}\ 0)_C$ plane, and $(1\ 1\ 1)_M$ is parallel to $(1\ 1\ \bar{4})_C$. Thus, it can be supposed that before the phase transformation reaction starts, the MWCNT physically adhered to the $(1\ 1\ \bar{2})_M$ plane (marked by the blue line in Figure 5d) of the layered Li_2MnO_3 via electrostatic heterocoagulation. During the thermal treatment for 0.5h, the interface is under the reduction effects driven by the MWCNTs, and phase transformation keeps progressing from surface toward the inner. However, because the interplanar distances of the paralleled crystal planes between the layered Li_2MnO_3 and the spinel $LiMn_2O_4$ do not match well with each other (From the zone axis $[\bar{1}\ 1\ 0]_{Monoclinic}$ for the layered Li_2MnO_3 and $[\bar{3}\ 0\ \bar{1}]_{Cubic}$ for the spinel $LiMn_2O_4$), the phase transformation proceeds at a relatively slow reaction rate during the thermal treatment. Thus, the complete spinel phase region transforms from the layered structure is less than 10 nm in wide.

When MWCNTs adhere to other exposed planes of the layered Li_2MnO_3 lattice, the phase transformation region may get larger in area. Figure 6 shows one of the cases. Phase transformation can be verified by the transformation of FTT patterns. Region A in Figure 6a reflects a mixed phase zone, which can be indexed to layered *C*2/*m* monoclinic lattice along the $[0\ 0\ 1]_M$ zone axis and spinel $Fd\bar{3}m$ cubic lattice along the $[1\ \bar{1}\ 2]_C$ zone axis. When approaching to the surface of the LR particle, like region B, the whole pattern can be indexed as spinel lattice, indicating the phase transformation is complete. The parallel relationships between the layered lattice and the spinel lattice $(1\ \bar{3}\ 0)_M \parallel (3\ 1\ 1)_C$ and $(2\ 0\ 0)_M \parallel (2\ \bar{2}\ 2)_C$ are revealed from the overlapping reflection spots in Figure 6b and statistics in Table S1 (Supporting Information). The lattice misfit rates are 2.38% and 2.22%, respectively, less than 5%, demonstrating that the transformed spinel phase retains a coherent lattice relationship with the layered parent component. Thus, the transformation does not require as much energy as that in the case in Figure 5, and the complete phase transformed zone stretches forward 15−20 nm from the surface to the inner. The edge of the mixed phase zone cannot be observed in Figure 6a because of the limited size of the HR-TEM image.

Based on the above discussion, it is revealed that the spinel modification phase comes from the Li_2MnO_3 phase, and the two phases are well compatible with each other in the lattice arrangement, which is beneficial for structure stability. Moreover, the phase transformation process relates to the crystal

DOI: 10.1021/am506354e
ACS Appl. Mater. Interfaces 2015, 7, 391−399

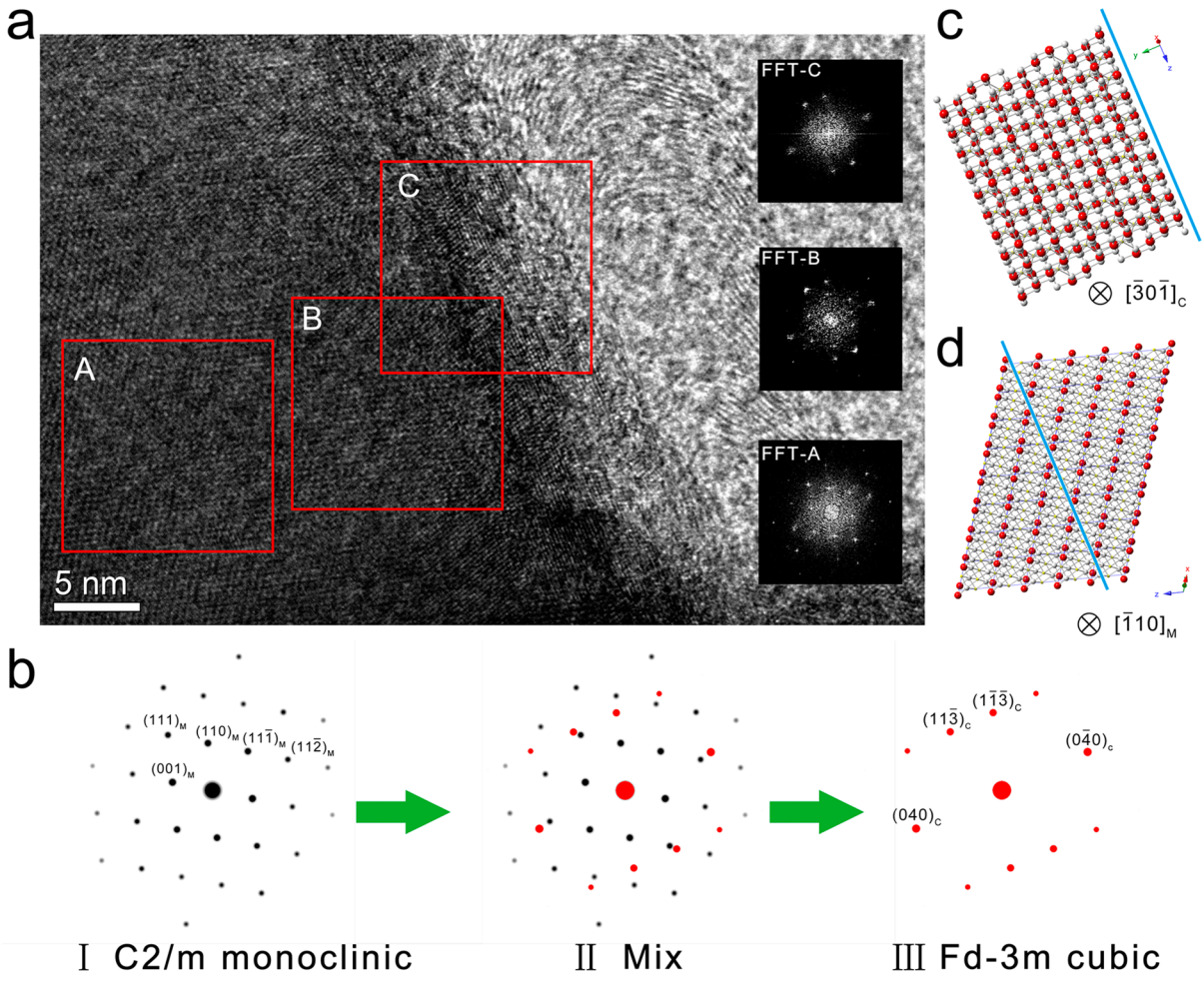

Figure 5. Interface between MWCNTs and LR, Case 1. (a) HR-TEM and FFT images of surface region of a LR particle where an MWCNT coagulates, (b) simulated diffraction patterns indicating the phase transformation process, (c) Cubic spinel phase viewed at $[\bar{3}\ 0\ \bar{1}]_C$, and (d) monoclinic layered phase viewed at $[\bar{1}\ 1\ 0]_M$. Red, yellow, and silvery atoms represent Mn, Li, and O atoms, respectively.

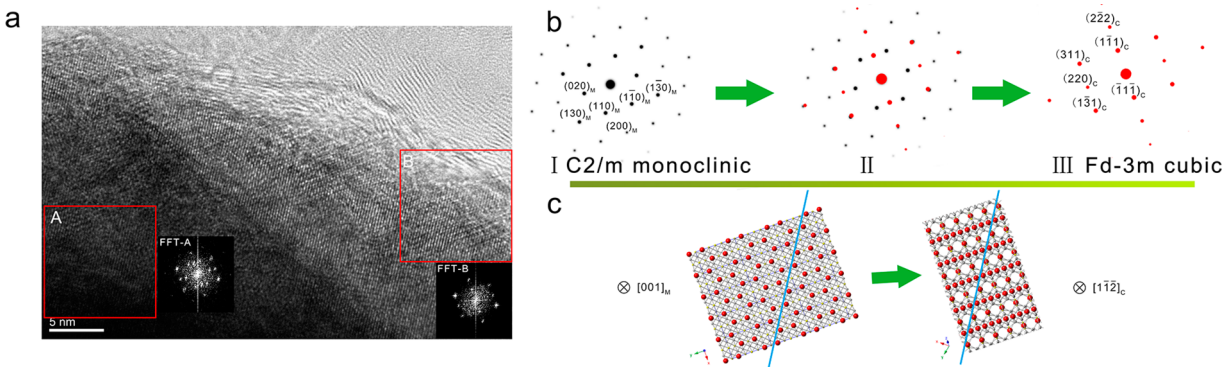

Figure 6. Interface between MWCNTs and LR, Case 2. (a) HR-TEM and FFT images of surface region of a LR particle where an MWCNT coagulates. (b) Simulated diffraction patterns indicating the phase transformation process. (c) Lattice model revealing phase transformation.

plane that the MWCNTs attach to, due to the different misfit between the interplanar distances of the paralleled crystal planes. The spinel phase transformation region will copy the morphology of the MWCNTs that coagulate on the LR clusters, stretching within the interface like a network, acting as a conductor for lithium and electrons, and supporting the structure of the original layered lattice.

3.3. Electrochemical Properties. *3.3.1. Initial Charge and Discharge Capacity.* Compared with the high theoretical capacity of LR, the spinel ionic network would not increase the capacity of the modified samples. Meanwhile, the MWCNT electric network hardly delivers any capacity as the cathode materials, and thus, the initial charge capacity should decrease linearly with the increasing amount of MWCNTs. However, the ionic and electronic double phase networks influence the dynamics. To be specific, the initial charge capacity of the LR samples contains two parts, as displayed in Figure 7a: the charge capacity contributed from the voltage below 4.5 V

DOI: 10.1021/am506354e
ACS Appl. Mater. Interfaces 2015, 7, 391−399

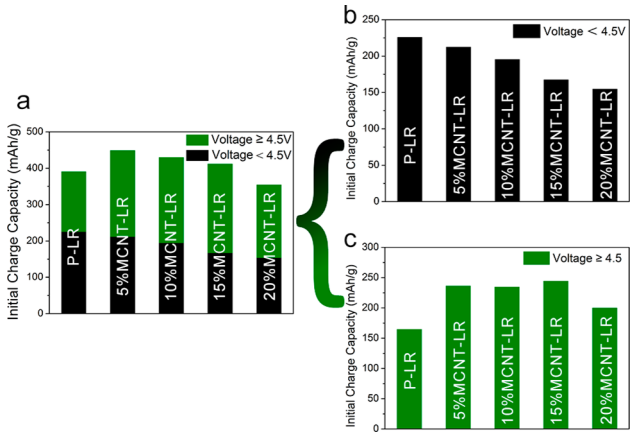

Figure 7. Histograms of initial charge capacity of samples before and after double phase network modification: (a) initial capacity at the voltage from 2.0 to 4.8 V, (b) initial capacity mainly attributed by $LiMO_2$ (M = Ni, Co, Mn), and (c) initial capacity mainly attributed by Li_2MnO_3 phase.

(mainly attributed by the $LiMO_2$ (M = Ni, Co, Mn) phase) and the charge capacity contributed from the voltage above 4.5 V (principally attributed by the Li_2MnO_3 phase).[6] In Figure 7b, the charge capacity by the $LiMO_2$ (M = Ni, Co, Mn) phase follows the linear decrease relationship with the increase of MWCNTs additives, indicating that the modification has no effect on the electrochemical behavior of $LiMO_2$ (M = Ni, Co, Mn) phase. The charge capacity by the Li_2MnO_3 phase in Figure 7c first increases, levels off, and then slightly declines with the increase of MWCNTs additives, indicating that the Li_2MnO_3 phase is deeply activated by the double phase modification. It is known that the irreversible capacity of LR materials mainly comes from the Li_2MnO_3 phase. Theoretically, 50% of the initial charge capacity of Li_2MnO_3 phase will become the irreversible capacity because of its electrochemical mechanism, which has been investigated in other research.[37] The more the Li_2MnO_3 phase is activated, the more the irreversible capacity will be, consistent with initial charge and discharge profiles at a low current rate of 0.05C (1C = 200 mA/g) (Figure S6, Supporting Information). Therefore, the double phase networks get more Li_2MnO_3 phase involved in the electrochemical reaction, leading to the decrease of the Coulombic efficiency with the contents of MWCNTs increase from 5% to 15% in mass.

3.3.2. Cycling Performance. The cycling performance is set from the 4th cycle at the current rate of 0.5C for 100 cycles (Figure 8a). The 1st (0.05C), 2nd (0.1C). and 3rd (0.2C) cycles are the activating procedures, which are not included in the cycling performance test. Although the initial discharge capacity of modified samples is lower than that of the pristine one (Figure S6, Supporting Information), better cycling performance is observed for modified samples. The capacity retention ratio after 100 cycles for P-LR, 5%MCNT-LR, 10% MCNT-LR, and 15%MCNT-LR are 93.3%, 96.3%, 92.3%, and 108.2%, respectively. (The capacity retention ratio equals the charge capacity at the 103rd cycle divided by the one at the 4th cycle.) The pristine LR only shows 183.1 mAh/g after 100 cycles. 15%MCNT-LR delivers a discharge capacity of 233.4 mAh/g in the 103rd cycle. From the aspect of electrochemistry, electrode polarization, owing to the poor kinetics, brings about the overgain and overloss of electron, leaving the active materials suffering from an over-reduction or overoxidation state. Both states are harmful to the stability of the active materials. Due to improvement effect on reaction kinetics, double phase networks reduce the polarization so that the modified LR materials can react under a more equilibrium state. Consequently, a better cycling stability can be achieved.

To look into the detailed transformation throughout the cycling process, the discharge curves of the 5th, 10th, 20th, 50th, and 103rd cycle are examined (Figure 8b). All the curves suffer a decay of the average discharge voltage, determined by the phase transformation from the layered $LiMnO_2$ to the spinel $LiMn_2O_4$, which cannot be tackled by surface modification method only.[4,38−40] Here, we investigate the open circuit voltage (OCV) when the state of charge (SOC) is 100%, simply defined as "discharge inception voltage". The discharge inception voltage of P-LR is only 4.00 V after 100 cycles while that of 15%MCNT-LR remains 4.66 V. On account of fast electron and lithium-ion transfer, the double phase networks can promote electrode reaction process and reduce the polarization, upgrading the discharge inception voltage.[36] Furthermore, throughout the cycling process, the discharge curves for P-LR consists of a group of slopes, no plateau observed. However, upon cycling, with more MWCNTs as a modification source, a longer plateau for double phase modified samples stretches more obviously at around 3 V, mainly corresponding to Mn^{4+}/Mn^{3+} of the spinel $LiMn_2O_4$.[41] Without double phase modification, lacking in reaction kinetics, the Li_2MnO_3 component tends to gradually change into spinel phase region by region. The highly single crystallized Li_2MnO_3 component transforms into a combination of spinel polycrystalline divided by crystal defects after cycling, and thus, both the voltage and the capacity keep decreasing during cycling process with no plateau appearing. But for modified samples, the lithium ion and electron can transfer through the surface in a leveled speed due to the double phase modification networks. The layered component can homogeneously transform into spinel phase in a more equilibrium state. Consequently, a great amount of highly ordered lithium rich layered region changes into highly ordered spinel area, so that the single-crystal character remains in the transformed region. Then, the plateau at 3 V well forms in the curve, and the modified samples, such as 15%MCNT-LR, possess optimized cycling performance.

3.3.3. Rate capability. Rate performances of samples before and after double phase modification are presented in Figure 8c. The test is set at different current rate of 0.2C, 0.5C, 1C, 2C, 5C, and returns to 0.2C. At a low current rate of 0.2C, the modified samples do not show much of an advantage over the pristine one. At the 1C rate, samples 5%MCNT-LR and 15% MCNT-LR still deliver a capacity of more than 210 mAh/g, while that for P-LR is only about 174 mAh/g. For even higher current rates such as 2C, all the double phase modified samples, benefited from ionic and electronic expressways on the surface region, deliver a much higher discharge capacity than the pristine one. Obviously, the P-LR sample can hardly be electrochemically activated at 5C, because the layered structure cannot afford such a highway for lithium and electrons transportation (Table S2, Supporting Information).[35,41−47] Meanwhile, the samples 5%MCNT-LR, 10%MCNT-LR, 15% MCNT-LR, and 20%MCNT-LR deliver a capacity of about 48, 114, 154, and 50 mAh/g at high rate of 5C, respectively. Undoubtedly, 15%MCNT-LR displays the best rate property. The sample of 20%MCNT-LR does not deliver the rate capability as outstanding as 10%MCNT-LR and 15%MCNT-

DOI: 10.1021/am506354e
ACS Appl. Mater. Interfaces 2015, 7, 391−399

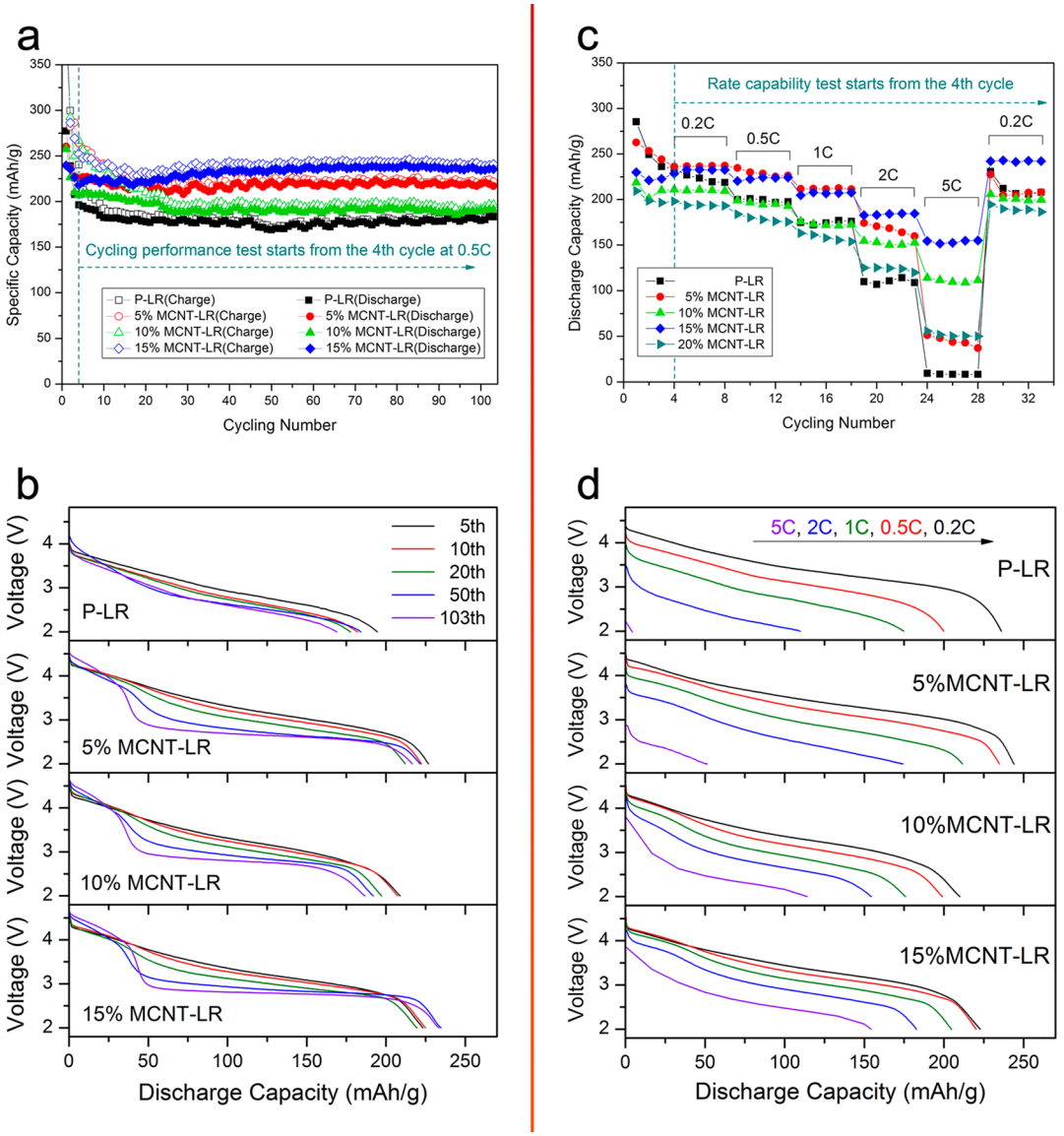

Figure 8. Electrochemical performance: (a) cycling performance at the current rate of 0.5C of the as-prepared LR samples before and after double phase modification, (b) discharging curves of the as-prepared LR samples at the 5th, 10th, 20th, 50th, and 103rd cycles for the cycling performance test, (c) rate capability of the as-prepared LR samples before and after double phase modification, (d) discharging curves of the as-prepared LR samples at various discharging current rates after charging at 0.2C rate to 4.8 V. For the overall electrochemical tests, the 1st (0.05C), 2nd (0.1C), and 3rd (0.2C) cycles are the activating procedures, which are not included in the cycling performance and rate capability test.

LR. Combined with the SEM images and the interface analysis, we can assume that the network morphology forms when the mass fractions of MWCNTs are ranging from 10% to 15%. When excess MWCNTs are added, such as 20%MCNT-LR in Figure 2h, the excess MWCNTs continue to coagulate on the surface of the well-arranged MWCNT network. First, without direct attachment to the active LR particles, the excess MWCNTs cannot effectively enhance the electronic conductivity and has no contribution to the spinel transformation (see Scheme S1 in the Supporting Information). Second, the excess MWCNTs prolong the lithium-ion pathway toward the active cathode. Third, as mentioned earlier, MWCNTs are not active materials as the cathode for LIBs. In turn, negative effects become stronger with the increase of the excess MWCNTs, resulting in the unsatisfactory rate capability of 20%MCNT-LR.

To observe the detailed distinctions of rate performance among samples before and after double phase modification, discharge curves at different current rates are displayed in Figure 8d. For P-LR sample, the discharge inception voltage decreases rapidly as the current rate increases (Figure S7, Supporting Information). The discharge curve at 5C appears rather short, due to the great polarization at high current density originated from the poor conductivity of the layered Li_2MnO_3 component segregating at the surface region of the LR particles (Figures 4, S4, and S5, Supporting Information). The polarization decreases energy efficiency and hinders electrochemical reactions of lithium ion batteries.[4] With the double phase network modification applied, the polarization at the high rate decreases as the content of MWCNTs increases from 5% to 15% in weight. For instance, 15%MCNT-LR can be discharged from the inception voltage of 3.87 V at 5C rate and presents the lowest surface resistances (Figure S8, Supporting Information), leading to the least polarization among all the tested samples.

DOI: 10.1021/am506354e
ACS Appl. Mater. Interfaces 2015, 7, 391−399

On the basis of the analysis on morphology, phase identification, the interface, and the electrochemical tests, the double phase modification mechanism is proposed (Scheme 1).

Scheme 1. Schematic Diagrams of Double Phase Network Modification Mechanism[a]

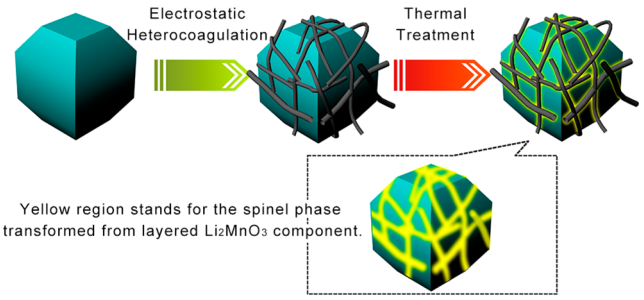

[a]The blue polyhedron represents the LR clusters. The gray tube represents MWCNTs. The yellow region represents spinel phase transformed from the layered Li_2MnO_3 component.

When an appropriate amount of MWCNTs, such as 15 wt %, adhere to the surface of LR particle particles, MWCNTs homogeneously disperse upon the surface of LR particles, forming a network for flexible electron transfer. No chemical reaction can take place between LR and MWCNTs during electrostatic coagulation due to the physical absorption process at room temperature. During the thermal treatment, MWCNTs show limited reducibility, owing to the relatively low holding temperature. Spinel phase transformation from layered component can only proceed at the interface between LR and MWCNTs. Thus, the spinel phase region will copy the morphology of attached MWCNTs. In this way, a network of ionic conductor is grounded at the surface region of the LR particles. At the same time, MWCNTs network can work as both trapper and conductor for electrons. Thus, as-formed double phase network modification enhances the electron and ionic conductivity at the same time, and significantly reduces the surface resistance. Furthermore, the unique spinel network has good compatibility with layered Li_2MnO_3 component, acting as a protector and a structure supporter. As a result, the double phase network modification decreases the surface resistance, reduces the polarization, and stabilizes the crystal structure.

4. CONCLUSION

A novel double phase network modification method has been systematically investigated. MWCNTs react with the surface-segregated Li_2MnO_3 phase in LR during short thermal treatment to yield an ionic conductive spinel phase, and thus, the spinel phase regions tend to copy the network morphology of MWCNTs, which attach to the LR particles. Moreover, the depth of phase transition zone depends on the driving force of phase transformation. The double phase network modification with both electronic and ionic conductivity significantly reduces the surface resistance and enhances the rate capability and the cycling performance of pristine $Li_{1.2}Co_{0.13}Ni_{0.13}Mn_{0.54}O_2$. As can be expected, the novel double phase network modification will show great potential in upgrading surface kinetics of lithium rich layered oxides.

■ ASSOCIATED CONTENT

Supporting Information

TEM images of the as-prepared modified LR, XRD patterns of the P-LR with thermal treatment at 300 °C under Ar protection and 15%MCNT-LR before thermal treatment, FESEM image of 15%MCNT-LR before thermal treatment, Raman spectrum, HR-TEM and FFT images of the surface regions of untreated LR, initial charge/discharge profiles, electrochemical impedance spectroscopy (EIS) profiles, tables of statistics for comparison. This material is available free of charge via the Internet at http://pubs.acs.org.

■ AUTHOR INFORMATION

Corresponding Authors

*N. Zhao. Email: nqzhao@tju.edu.cn.
*E. Liu. Email: ezliu@tju.edu.cn.

Notes

The authors declare no competing financial interest.

■ ACKNOWLEDGMENTS

This work was supported by the Key Technologies R & D program of Tianjin (12ZCZDGX00800), the National Natural Science Foundation of China (Grant No. 11474216), China-EU Science and Technology Cooperation Project (No. 1206), and the Innovation Foundation of Tianjin University.

■ REFERENCES

(1) Thackeray, M. M.; Wolverton, C.; Isaacs, E. D. Electrical Energy Storage for Transportation—Approaching the Limits of, and Going beyond, Lithium-Ion Batteries. *Energy Environ. Sci.* **2012**, *5*, 7854–7863.
(2) Yu, H.; Zhou, H. High-Energy Cathode Materials (Li_2MnO_3–$LiMO_2$) for Lithium-Ion Batteries. *J. Phys. Chem. Lett.* **2013**, *4*, 1268–1280.
(3) Cheng, F.; Liang, J.; Tao, Z.; Chen, J. Functional Materials for Rechargeable Batteries. *Adv. Mater.* **2011**, *23*, 1695–1715.
(4) Kim, T.-H.; Park, J.-S.; Chang, S. K.; Choi, S.; Ryu, J. H.; Song, H.-K. The Current Move of Lithium Ion Batteries towards the Next Phase. *Adv. Energy Mater.* **2012**, *2*, 860–872.
(5) Lu, W.; Wu, Q.; Dees, D. W. Electrochemical Characterization of Lithium and Manganese Rich Composite Material for Lithium Ion Batteries. *J. Electrochem. Soc.* **2013**, *160*, A950–A954.
(6) Kang, S. H.; Johnson, C. S.; Vaughey, J. T.; Amine, K.; Thackeray, M. M. The Effects of Acid Treatment on the Electrochemical Properties of 0.5 Li_2MnO_3·0.5 $LiNi_{0.44}Co_{0.25}Mn_{0.31}O_2$ Electrodes in Lithium Cells. *J. Electrochem. Soc.* **2006**, *153*, A1186–A1192.
(7) Chen, Z.; Qin, Y.; Amine, K.; Sun, Y. K. Role of Surface Coating on Cathode Materials for Lithium-Ion Batteries. *J. Mater. Chem.* **2010**, *20*, 7606–7612.
(8) He, W.; Qian, J.; Cao, Y.; Ai, X.; Yang, H. Improved Electrochemical Performances of Nanocrystalline Li-$[Li_{0.2}Mn_{0.54}Ni_{0.13}Co_{0.13}]O_2$ Cathode Material for Li-Ion Batteries. *RSC Adv.* **2012**, *2*, 3423–3429.
(9) Kang, S.; Thackeray, M. M. Enhancing the Rate Capability of High Capacity $xLi_2MnO_3 \cdot (1-x)LiMO_2$ (M = Mn, Ni, Co) Electrodes by Li-Ni-PO_4 Treatment. *Electrochem. Commun.* **2009**, *11*, 748–751.
(10) Shi, S. J.; Tu, J. P.; Tang, Y. Y.; Liu, X. Y.; Zhang, Y. Q.; Wang, X. L.; Gu, C. D. Enhanced Cycling Stability of Li-$[Li_{0.2}Mn_{0.54}Ni_{0.13}Co_{0.13}]O_2$ by Surface Modification of MgO with Melting Impregnation Method. *Electrochim. Acta* **2013**, *88*, 671–679.
(11) Shi, S. J.; Tu, J. P.; Zhang, Y. J.; Zhang, Y. D.; Zhao, X. Y.; Wang, X. L.; Gu, C. D. Effect of Sm_2O_3 Modification on Li-$[Li_{0.2}Mn_{0.56}Ni_{0.16}Co_{0.08}]O_2$ Cathode Material for Lithium Ion Batteries. *Electrochim. Acta* **2013**, *108*, 441–448.

DOI: 10.1021/am506354e
ACS Appl. Mater. Interfaces 2015, 7, 391–399

(12) Wang, Q. Y.; Liu, J.; Murugan, A. V.; Manthiram, A. High Capacity Double-Layer Surface Modified $Li[Li_{0.2}Mn_{0.54}Ni_{0.13}Co_{0.13}]O_2$ Cathode with Improved Rate Capability. *J. Mater. Chem.* **2009**, *19*, 4965−4972.
(13) Wu, F.; Li, N.; Su, Y.; Shou, H.; Bao, L.; Yang, W.; Zhang, L.; An, R.; Chen, S. Spinel/Layered Heterostructured Cathode Material for High-Capacity and High-Rate Li-Ion Batteries. *Adv. Mater.* **2013**, *25*, 3722−3726.
(14) Liu, J.; Wang, Q.; Reeja-Jayan, B.; Manthiram, A. Carbon-Coated High Capacity Layered $Li[Li_{0.2}Mn_{0.54}Ni_{0.13}Co_{0.13}]O_2$ Cathodes. *Electrochem. Commun.* **2010**, *12*, 750−753.
(15) Su, L.; Jing, Y.; Zhou, Z. Li Ion Battery Materials with Core-Shell Nanostructures. *Nanoscale* **2011**, *3*, 3967−3983.
(16) Marcinek, M. L.; Wilcox, J. W.; Doeff, M. M.; Kostecki, R. M. Microwave Plasma Chemical Vapor Deposition of Carbon Coatings on $LiNi_{1/3}Co_{1/3}Mn_{1/3}O_2$ for Li-Ion Battery Composite Cathodes. *J. Electrochem. Soc.* **2009**, *156*, A48−A51.
(17) Li, H.; Zhou, H. Enhancing the Performances of Li-Ion Batteries by Carbon-Coating: Present and Future. *Chem. Commun.* **2012**, *48*, 1201−1217.
(18) Jiang, K.; Wu, X.; Yin, Y.; Lee, J.; Kim, J.; Guo, Y. Superior Hybrid Cathode Material Containing Lithium-Excess Layered Material and Graphene for Lithium-Ion Batteries. *ACS Appl. Mater. Interfaces* **2012**, *4*, 4858−4863.
(19) Deng, Y.; Liu, S.; Liang, X. Study of Carbon Surface-Modified $Li[Li_{0.2}Mn_{0.54}Ni_{0.13}Co_{0.13}]O_2$ for High-Capacity Lithium Ion Battery Cathode. *J. Solid State Electrochem.* **2013**, *17*, 1067−1075.
(20) Song, B.; Lai, M. O.; Liu, Z.; Liu, H.; Lu, L. Graphene-based Surface Modification on Layered Li-Rich Cathode for High-Performance Li-Ion Batteries. *J. Mater. Chem. A* **2013**, *1*, 9954−9965.
(21) Song, B.; Liu, H.; Liu, Z.; Xiao, P.; Lai, M.; Lu, L. High Rate Capability Caused by Surface Cubic Spinels in Li-Rich Layer-Structured Cathodes for Li-Ion Batteries. *Sci. Rep.* **2013**, *3*, DOI: 10.1038/srep03094.
(22) Ban, C.; Li, Z.; Wu, Z.; Kirkham, M. J.; Chen, L.; Jung, Y. S.; Payzant, E. A.; Yan, Y.; Whittingham, M. S.; Dillon, A. C. Extremely Durable High-Rate Capability of a $LiNi_{0.4}Mn_{0.4}Co_{0.2}O_2$ Cathode Enabled with Single-Walled Carbon Nanotubes. *Adv. Energy Mater.* **2011**, *1*, 58−62.
(23) López-Maldonado, E. A.; Oropeza-Guzman, M. T.; Jurado-Baizaval, J. L.; Ochoa-Terán, A. Coagulation-Flocculation Mechanisms in Wastewater Treatment Plants through Zeta Potential Measurements. *J. Hazard. Mater.* **2014**, *279*, 1−10.
(24) Li, Y.; Yin, D.; Wang, Z.; Li, B.; Xue, G. Controlling the Heterocoagulation Process for Fabricating PS-$CoFe_2O_4$ Nanocomposite Particles. *Colloids Surf., A* **2009**, *339*, 100−105.
(25) Sheem, K. Y.; Sung, M.; Lee, Y. H. Electrostatic Heterocoagulation of Carbon Nanotubes and $LiCoO_2$ Particles for a High-Performance Li-Ion Cell. *Electrochim. Acta* **2010**, *55*, 5808−5812.
(26) Li, R.; Yang, X.; Li, G.; Li, S.; Huang, W. Core−Corona Polymer Composite Particles by Self-Assembled Heterocoagulation Based on a Hydrogen-Bonding Interaction. *Langmuir* **2006**, *22*, 8127−8133.
(27) Thackeray, M. M.; Kang, S.; Johnson, C. S.; Vaughey, J. T.; Benedek, R.; Hackney, S. A. Li_2MnO_3-Stabilized $LiMO_2$ (M = Mn, Ni, Co) Electrodes for Lithium-Ion Batteries. *J. Mater. Chem.* **2007**, *17*, 3112−3125.
(28) Strobel, P.; Lambert-Andron, B. Crystallographic and Magnetic Structure of Li_2MnO_3. *J. Solid State Chem.* **1988**, *75*, 90−98.
(29) Wang, C.; Jarvis, K. A.; Ferreira, P. J.; Manthiram, A. Effect of Synthesis Conditions on the First Charge and Reversible Capacities of Lithium-Rich Layered Oxide Cathodes. *Chem. Mater.* **2013**, *25*, 3267−3275.
(30) Wills, A. S.; Raju, N. P.; Greedan, J. E. Low-Temperature Structure and Magnetic Properties of the Spinel $LiMn_2O_4$: A Frustrated Antiferromagnet and Cathode Material. *Chem. Mater.* **1999**, *11*, 1510−1518.
(31) Chung, H.; Myung, S.; Cho, T.; Son, J. Lattice Parameter as a Measure of Electrochemical Properties of $LiMn_2O_4$. *J. Power Sources* **2001**, *97*−*98*, 454−457.
(32) Johnson, C. S.; Li, N.; Lefief, C.; Vaughey, J. T.; Thackeray, M. M. Synthesis, Characterization and Electrochemistry of Lithium Battery Electrodes: $xLi_2MnO_3\cdot(1-x)LiMn_{0.333}Ni_{0.333}Co0.333O_2$ ($0 \le x \le 0.7$). *Chem. Mater.* **2008**, *20*, 6095−6106.
(33) Martha, S. K.; Nanda, J.; Veith, G. M.; Dudney, N. J. Electrochemical and Rate Performance Study of High-Voltage Lithium-Rich Composition: $Li_{1.2}Mn_{0.525}Ni_{0.175}Co_{0.1}O_2$. *J. Power Sources* **2012**, *199*, 220−226.
(34) Croy, J. R.; Kim, D.; Balasubramanian, M.; Gallagher, K.; Kang, S.; Thackeray, M. M. Countering the Voltage Decay in High Capacity $xLi_2MnO_3\cdot(1\text{-}x)LiMO_2$ Electrodes (M=Mn, Ni, Co) for Li^+-Ion Batteries. *J. Electrochem. Soc.* **2012**, *159*, A781−A790.
(35) Shen, C.; Huang, L.; Lin, Z.; Shen, S.; Wang, Q.; Su, H.; Fu, F.; Zheng, X. Kinetics and Structural Changes of Li-Rich Layered Oxide $0.5Li_2MnO_3\cdot0.5LiNi_{0.292}Co_{0.375}Mn_{0.333}O_2$ Material Investigated by a Novel Technique Combining in Situ XRD and a Multipotential Step. *ACS Appl. Mater. Interfaces* **2014**, *15*, 13271−13279.
(36) Islam, M. S.; Fisher, C. A. J. Lithium and Sodium Battery Cathode Materials: Computational Insights into Voltage, Diffusion and Nanostructural Properties. *Chem. Soc. Rev.* **2014**, *43*, 185−204.
(37) Johnson, C. S.; Li, N.; Lefief, C.; Thackeray, M. M. Anomalous Capacity and Cycling Stability of $xLi_2MnO_3\cdot(1\text{ - }x)LiMO_2$ Electrodes (M = Mn, Ni, Co) in Lithium Batteries at 50 °C. *Electrochem. Commun.* **2007**, *9*, 787−795.
(38) Luo, D.; Li, G.; Fu, C.; Zheng, J.; Fan, J.; Li, Q.; Li, L. A New Spinel-Layered Li-Rich Microsphere as a High-Rate Cathode Material for Li-Ion Batteries. *Adv. Energy Mater.* **2014**, *4*, DOI: 10.1002/aenm.201400062.
(39) Lee, E.; Huq, A.; Chang, H.; Manthiram, A. High-Voltage, High-Energy Layered-Spinel Composite Cathodes with Superior Cycle Life for Lithium-Ion Batteries. *Chem. Mater.* **2012**, *24*, 600−612.
(40) Jung, S.; Gwon, H.; Hong, J.; Park, K.; Seo, D.; Kim, H.; Hyun, J.; Yang, W.; Kang, K. Understanding the Degradation Mechanisms of $LiNi_{0.5}Co_{0.2}Mn_{0.3}O_2$ Cathode Material in Lithium Ion Batteries. *Adv. Energy Mater.* **2014**, *4*, DOI: 10.1002/aenm.201300787.
(41) Johnson, C. S.; Li, N.; Vaughey, J. T.; Hackney, S. A.; Thackeray, M. M. Lithium-Manganese Oxide Electrodes with Layered-Spinel Composite Structures $xLi_2MnO_3\cdot(1\text{-}x)Li_{1+y}Mn_{2-y}O_4$ ($0 < x < 1$, $0 \le y \le 0.33$) for Lithium Batteries. *Electrochem. Commun.* **2005**, *7*, 528−536.
(42) Eftekhari, A. Electrochemical Behavior of Thin-Film $LiMn_2O_4$ Electrode in Aqueous Media. *Electrochim. Acta* **2001**, *47*, 495−499.
(43) Li, Z.; Du, F.; Bie, X.; Zhang, D.; Cai, Y.; Cui, X.; Wang, C.; Chen, G.; Wei, Y. Electrochemical Kinetics of the Li-$[Li_{0.23}Co_{0.3}Mn_{0.47}]O_2$ Cathode Material Studied by GITT and EIS. *J. Phys. Chem. C* **2010**, *114*, 22751−22757.
(44) Zheng, W.; Xu, X.; Cheng, L.; Shui, M.; Shu, J.; Gao, S.; Lu, Z.; Feng, L.; Ren, Y. The Intercalation/Deintercalation Kinetic Studies on the Structure-Integrated Cathode Material $0.5Li_2MnO_3$ $0.5LiNi_{0.5}Mn_{0.5}O_2$. *Ionics* **2013**, *19*, 1509−1514.
(45) Lin, J.; Mu, D.; Jin, Y.; Wu, B.; Ma, Y.; Wu, F. Li-Rich Layered Composite $Li[Li_{0.2}Ni_{0.2}Mn_{0.6}]O_2$ Synthesized by a Novel Approach as Cathode Material for Lithium Ion Battery. *J. Power Sources* **2013**, *230*, 76−80.
(46) Bai, Y.; Wang, X.; Zhang, X.; Shu, H.; Yang, X.; Hu, B.; Wei, Q.; Wu, H.; Song, Y. The Kinetics of Li-Ion Deintercalation in the Li-Rich Layered $Li_{1.12}[Ni_{0.5}Co_{0.2}Mn_{0.3}]_{0.89}O_2$ Studied by Electrochemical Impedance Spectroscopy and Galvanostatic Intermittent Titration Technique. *Electrochim. Acta* **2013**, *109*, 355−364.
(47) Takai, S.; Yoshioka, K.; Iikura, H.; Matsubayashi, M.; Yao, T.; Esaka, T. Tracer Diffusion Coefficients of Lithium Ion in $LiMn_2O_4$ Measured by Neutron Radiography. *Solid State Ionics* **2014**, *256*, 93−96.

DOI: 10.1021/am506354e
ACS Appl. Mater. Interfaces 2015, 7, 391−399